

PCCCP

Physical Chemistry Chemical Physics

Accepted Manuscript

This article can be cited before page numbers have been issued, to do this please use: L. J. Duarte, C. M. Nunes, A. A. C. Braga, R. Fausto and A. J. Lopes Jesus, *Phys. Chem. Chem. Phys.*, 2026, DOI: 10.1039/D5CP04677G.



This is an Accepted Manuscript, which has been through the Royal Society of Chemistry peer review process and has been accepted for publication.

Accepted Manuscripts are published online shortly after acceptance, before technical editing, formatting and proof reading. Using this free service, authors can make their results available to the community, in citable form, before we publish the edited article. We will replace this Accepted Manuscript with the edited and formatted Advance Article as soon as it is available.

You can find more information about Accepted Manuscripts in the [Information for Authors](#).

Please note that technical editing may introduce minor changes to the text and/or graphics, which may alter content. The journal's standard [Terms & Conditions](#) and the [Ethical guidelines](#) still apply. In no event shall the Royal Society of Chemistry be held responsible for any errors or omissions in this Accepted Manuscript or any consequences arising from the use of any information it contains.

NIR Excitation-Driven Conformational Isomerizations of Thymol and Carvacrol Isolated in a Nitrogen Cryomatrix

Leonardo J. Duarte,^{a,b,c*} Cláudio M. Nunes,^c Atualpa A. C. Braga,^a R. Fausto^{c,d} and A. J. Lopes Jesus^{e*}

^a Institute of Chemistry, Department of Fundamental Chemistry, University of São Paulo, 05508-900, São Paulo, Brazil

^b Center for Natural and Human Sciences, Federal University of ABC, 09280-560, Santo André, SP, Brazil

^c University of Coimbra, CQC-IMS, Department of Chemistry, 3004-535, Coimbra, Portugal

^d Spectroscopy@IKU, Faculty Sciences and Letters, Department of Physics, Istanbul Kultur University, Bakirkoy, Istanbul 34158, Turkey

^e University of Coimbra, CQC-IMS, Faculty of Pharmacy, 3004-295, Coimbra, Portugal

Abstract

Thymol (2-isopropyl-5-methylphenol) and carvacrol (5-isopropyl-2-methylphenol) differ only in the relative positions of the hydroxyl and alkyl substituents, yet this subtle change reverses their torsional energy profiles: in thymol, isopropyl rotation is more hindered than OH torsion, whereas in carvacrol the opposite occurs. These features make the two compounds ideal model systems to investigate how differences in OH and isopropyl torsional barriers influence the redistribution of vibrational energy following near-infrared (NIR) excitation of the 2νOH overtone. Monomers of both compounds were isolated in a nitrogen matrix at 15 K and irradiated within the profile of the 2νOH overtone band (7110 to 7060 cm⁻¹) by using tunable laser light. Spectroscopic monitoring revealed selective and bidirectional interconversion between rotamers differing in the OH orientation. On the contrary, no interconversion between conformers differing in the isopropyl orientation was observed. This is particularly noteworthy for carvacrol, as its isopropyl torsional barrier is comparable in magnitude to that of the OH rotation. These findings support OH-rotamerization as the main route for vibrational energy redistribution, independent of the relative barrier heights. The photogenerated higher-energy cis-OH rotamers were observed to relax spontaneously to their trans counterparts via intramolecular hydrogen-atom tunneling, whose kinetics were quantitatively determined.

* Corresponding authors: Leonardo J. Duarte; A. J. Lopes Jesus

E-mail addresses: ljduarte@iq.usp.br; ajorge@ff.uc.pt



1. INTRODUCTION

Since the groundbreaking work of Pettersson, Lundell, Khriachtchev and Räsänen in the late 1990s, which demonstrated the narrowband Near Infrared (NIR) induced rotamerization of formic acid under matrix-isolation conditions¹, the combination of NIR laser sources with the matrix-isolation technique has emerged as a powerful tool for triggering, in a very selective way, conformational transformations in a wide variety of molecules. Carboxylic acids have been extensively studied systems^{2–18}, though many other types of molecules have also been examined. These include the Kojic¹⁹ and squaric²⁰ acids, aminoacids^{21–24}, nucleobases and their derivatives^{25–27}, phenol and indole derivatives^{28–31}, among other species^{32–36}. Comprehensive reviews have also been published, highlighting key achievements and advances in the field^{37–41}.

Vibrationally-induced conformational transformations are fundamentally controlled by Intramolecular Vibrational Energy Redistribution (IVR)^{42–46}, wherein relaxation following excitation of, for example, OH, CH, NH, or NH₂ stretching vibrations, or their combinations and overtones, leads to a transfer of energy to a reactive torsional coordinate, resulting in the conformational change. For rotamerization to occur under NIR excitation, the deposited vibrational energy should typically exceed the torsional barrier. However, IVR can sometimes promote conformational changes even when the initially excited vibrational mode lies below this threshold⁴⁷. The mechanism behind this process is still a matter of debate in the literature. Based on the experimentally observed isomerization of formic acid triggered by the excitation of normal modes below the barrier, Pettersson *et al.* proposed that the mechanism must involve tunneling effects⁴⁷. In a recent theoretical study from our laboratory on HONO isomerization, we found a similar mechanism, suggesting that IR-induced isomerization below the barrier may occur via tunneling assisted IVR⁴⁸.

For OH-containing molecules, excitation of the first overtone of an OH stretching mode (2νOH) often couples strongly with the torsional motion of the same OH group^{6,15,47}. Nevertheless, various studies have shown that excitation of a 2νOH mode can also drive the rotation of heavier molecular groups^{4,8,21,30,47}. Two illustrative examples are 3-hydroxy-2-formyl-azirine⁴⁹ and kojic acid¹⁹ in which excitation of the 2νOH overtones was found to induce conformational changes in the heavy hydroxymethyl and formyl fragments, respectively (**Figure 1**). Investigation of the



interplay between OH rotamerization and other conformational IVR redistribution pathways under matrix-isolation conditions is difficult when noble gases are used as matrix hosts, since the high-energy OH rotamers generated by IR excitation tend to relax rapidly to lower-energy forms via H-tunneling^{1,2,15,20,22,50}. In contrast, when N₂ is used as host matrix, a significant enhancement of the life-time of these high-energy OH rotamers^{8,20,51} occurs, through the formation of OH...N₂ interactions^{52,53}. This provides a more favorable environment for evaluating the efficiency of the NIR-induced OH torsional motions in comparison with other competing conformational rearrangements.

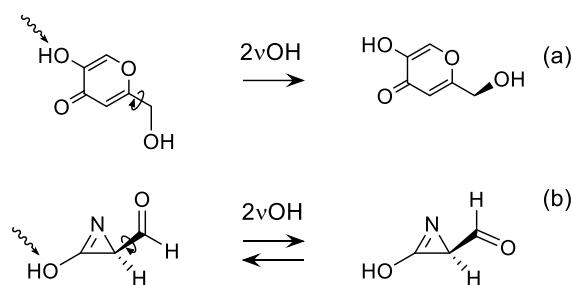


Figure 1. Illustrative examples of rotamerization of heavy-atom fragments triggered by NIR excitation of $2\nu_{\text{OH}}$ overtones of (a) kojic acid and (b) 3-hydroxy-2-formyl-azirine.

As part of a series of studies conducted in our laboratory on the NIR-induced isomerization of phenol derivatives bearing an isopropyl group attached to the phenyl ring, we investigated whether this group could undergo rotation upon excitation of the overtone of an OH stretch vibration. The model systems selected for this purpose were thymol (2-isopropyl-5-methylphenol) and carvacrol (5-isopropyl-2-methylphenol), whose structures are depicted in **Figure 2**. In low-temperature noble gas matrices (Ar and Xe), the two lowest-energy conformers having the OH group pointing away from the nearest alkyl fragment (trans-OH, **Figure 3**) and differing in the orientation of the isopropyl fragment, were spectroscopically identified^{54,55}. In contrast, the higher-energy conformers, with the OH group oriented toward the nearest alkyl fragment (cis-OH, **Figure 3**), were not detected due to their fast relaxation via H-tunneling rotamerization into the more stable trans-OH counterparts. Such behavior is consistent with previous observations for other structurally related phenol derivatives in noble gas matrices^{28,29,54–56}.

The conformational landscapes of thymol and carvacrol have also been investigated in the gas phase using broadband microwave spectroscopy^{57,58} and laser-based jet techniques⁵⁹. These



studies enabled the identification of multiple conformers with high structural precision. These included the lowest-energy structures in which the OH group is oriented away from the nearest alkyl substituent, which were also identified in our previous studies in Ar and Xe matrices^{54,55}. Besides, higher-energy conformers in which the OH group points toward the alkyl fragment were also identified: one such conformer in thymol and two in carvacrol. Gas-phase approaches thus provide detailed insight into intrinsic molecular structures and relative conformer energetics under isolated, collision-free conditions, although the investigation of long-timescale conformational dynamics is challenging. In contrast, matrix-isolation infrared spectroscopy offers a complementary framework for investigating conformational interconversions over extended timescales, providing access to dynamical information that complements the structural insights obtained from gas-phase jet experiments.

Attempts to induce interconversion between the two trans-OH conformers (via rotation of the isopropyl group) using narrowband NIR light tuned to the $2\nu_{\text{OH}}$ vibration were performed for thymol isolated in a Xe matrix. Despite the energy deposited in the molecule by the NIR radiation ($7061\text{-}7047\text{ cm}^{-1}$, equivalent to $\sim 84\text{ kJ mol}^{-1}$) being more than three times higher than the computed isopropyl rotamerization barrier ($23\text{-}26\text{ kJ mol}^{-1}$, **Figure 3**), no interconversion between the two conformers was observed⁵⁵. We hypothesized that this lack of interconversion arises from preferential dissipation of vibrational energy into the OH torsional mode, whose calculated barrier is considerably lower than that for isopropyl rotation ($9\text{-}14\text{ kJ mol}^{-1}$, **Figure 3**). To further investigate this hypothesis, the present study aims to obtain deeper insight into the mechanisms governing conformational transformations in thymol and carvacrol isolated in an N_2 matrix. Importantly, the isopropyl rotamerization barrier in carvacrol ($10\text{-}11\text{ kJ mol}^{-1}$) is significantly lower than in thymol and is of the same order as the OH-rotamerization barrier ($11\text{-}13\text{ kJ mol}^{-1}$, **Figure 3**). Therefore, these molecular systems offer a valuable opportunity to evaluate whether the efficiency of NIR-induced rotamerization is dictated primarily by the barrier height or not.

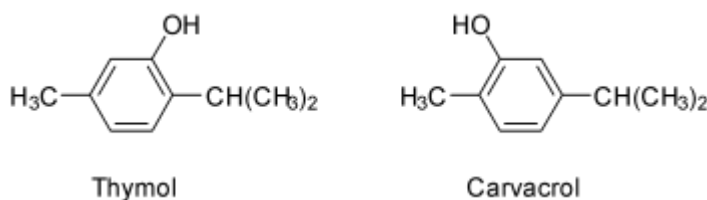


Figure 2. Molecular structures of thymol (2-isopropyl-5-methylphenol) and carvacrol (5-isopropyl-2-methylphenol).

In addition to the selective NIR-induced conformational interconversions, the kinetics of the spontaneous cis-to-trans OH conversion in a N₂ matrix under dark conditions were investigated for both compounds. This process is mediated by intramolecular hydrogen-atom tunneling through the rotational barrier. By tracking the temporal evolution of diagnostic vibrational bands, the depopulation rates of the cis-OH conformers and the associated tunneling dynamics were quantitatively characterized.

2. METHODS

2.1. Experimental Section

Solid thymol (Fluka, 99.5%), liquid carvacrol (Sigma-Aldrich, 98%), and high-purity nitrogen (Air Liquide, N50) were used in the experiments. A detailed description of the procedure and equipment used in the matrix deposition is provided elsewhere^{54,55}. IR spectra of the matrix-isolated compounds were recorded with a Thermo Nicolet 6700 Fourier-transform infrared (FTIR) spectrometer both in the mid-IR (4000–400 cm⁻¹) and NIR (7500–4000 cm⁻¹) regions. In the mid-IR region, the spectra were recorded with a 0.5 cm⁻¹ resolution using a deuterated triglycine sulphate (DTGS) detector and a KBr beam splitter. In the NIR region, the spectra were recorded with 1 cm⁻¹ resolution using an InGaAs detector and a CaF₂ beam splitter. The NIR irradiations were undertaken *in situ* using the idle beam of a Spectra Physics Quanta-Ray optical parametric oscillator (MOPO-SL) pumped by a Nd:YAG Spectra Physics Quanta-Ray PRO-230-10 laser, providing a NIR beam with a bandwidth of 0.2 cm⁻¹, pulse frequency of 10 Hz, and an energy of ~10 mJ. The time of irradiation at a particular wavenumber was ~20 min. In some experiments, to partially protect the matrices from the high frequency broadband radiation emitted from the IR spectrometer, a longpass filter (Edmund Optics) transmitting only IR light below ~2200 cm⁻¹ was used. Complete blocking of IR light (dark conditions) was achieved by placing a metal plate between the spectrometer source and the sample.

2.2. Theoretical Calculations



To assist in the interpretation of the experimental IR spectra, harmonic vibrational calculations at the B3LYP^{60–63}/6-311++G(d,p) level were performed for the conformers of thymol and carvacrol, using fully optimized geometries at the same level of theory. The computed harmonic wavenumbers were scaled by 0.980 and 0.945 for the regions below and above 2000 cm⁻¹, respectively. Despite the relative simplicity of this combination of functional and basis set, it has been successfully employed in our laboratory to predict the vibrational spectra of these molecules, and the calculated conformational energies compare well with those obtained at higher levels of theory, as demonstrated in our previous studies on these molecules^{54,55}. Anharmonic vibrational calculations at the B3LYP/6-311++G(2d,2p) were also carried out using the fully automated second-order vibrational perturbative approach developed by Barone and co-workers^{64–66}. Calculated anharmonic wavenumbers were not scaled. All calculations were performed using the Gaussian 16 program package (Rev. B.01)⁶⁷.

3. RESULTS AND DISCUSSION

3.1. Gas-Phase Conformational Distribution and Barriers for the Hydroxyl and Isopropyl Rotamerizations

The molecular structures of carvacrol and thymol are shown in **Figure 2**. They differ only by the position of the OH group relative to the alkyl fragments: in thymol it is ortho to the isopropyl group, whereas in carvacrol it is ortho to the methyl group. The conformational behavior of both molecules has been extensively studied in our laboratory using various levels of theory^{54,55}. Here, we highlight only the key findings from these studies that are relevant to the present work.

Both molecules can adopt four distinct conformers, each designated by a two-letter code (**Figure 3**). The first letter denotes the orientation of the tertiary C–H bond of the isopropyl fragment relative to the C–O bond, while the second indicates the orientation of the OH group relative to the nearest alkyl fragment. The notation used is as follows: **g** (gauche, ~60°), **c** (cis, 0°), and **t** (trans, 180°). The relative Gibbs energies of the conformers at 298.15 K, calculated at the B3LYP/6-311++G(d,p) level, and the corresponding Boltzmann populations, are included in **Figure 3**. From these data, the following conclusions can be drawn: (i) for the two molecules, the two trans-OH conformers (**gt** and **tt** in thymol; **tt** and **ct** in carvacrol) are more stable than their cis-OH counterparts (**gc** and **tc** in thymol; **tc** and **cc** in carvacrol); (ii) within each group of



conformers, thymol shows a preference for the gauche orientation of the C–H bond over a trans one (the cis conformation is not a minimum). In carvacrol, however, the cis and trans orientations of the C–H bond are practically isoenergetic. According to the gas-phase population predictions at 298.15 K (also included in **Figure 3**), thymol exists predominantly in the **gt** conformer, followed by **tt**, with a minor contribution from **gc** and a residual presence of **tc**. In contrast, carvacrol exhibits a broader conformational distribution, with the **tt** and **ct** forms being the most abundant and nearly equimolar, but the **tc** and **cc** conformers also contribute appreciably. These results are consistent with those reported by Schmitz et al⁶⁸.

In addition to gas-phase population predictions, the energy barriers for conformational isomerization, included in **Figure 3**, play a crucial role in determining which conformers may persist upon matrix deposition. The barriers for OH rotamerization range from 11 to 14 kJ mol⁻¹ for the conversion of the trans-OH into the cis-OH conformers and from 9 to 12 kJ mol⁻¹ for the reverse process. These barriers are sufficiently high to suppress conventional, temperature-dependent over-the-barrier relaxation in a cryogenic matrix. Nevertheless, because the OH-rotamerization involves the motion of a light hydrogen atom, H-tunneling can promote cis-OH → trans-OH decay. This tunneling pathway accounts for the absence of detectable cis-OH conformers of thymol and carvacrol in noble-gas matrices, where they are assumed to relax too rapidly to be observed spectroscopically^{54,55}. By contrast, owing to the well-known stabilizing effect of N₂ as a matrix medium, the higher energy cis-OH conformers are more likely to be detected in N₂ matrices. Regarding the isopropyl group rotamerization, the calculated energy barriers range from 23 to 26 kJ mol⁻¹ in thymol and are significantly lower in carvacrol (10–11 kJ mol⁻¹), where the increased spatial separation between the isopropyl and OH groups reduce steric hindrance. From an experimental perspective, such energy barriers, involving the movement of a bulky fragment, cannot be overcome at cryogenic temperatures (10–20 K), effectively preventing interconversion between these conformers under matrix isolation conditions.



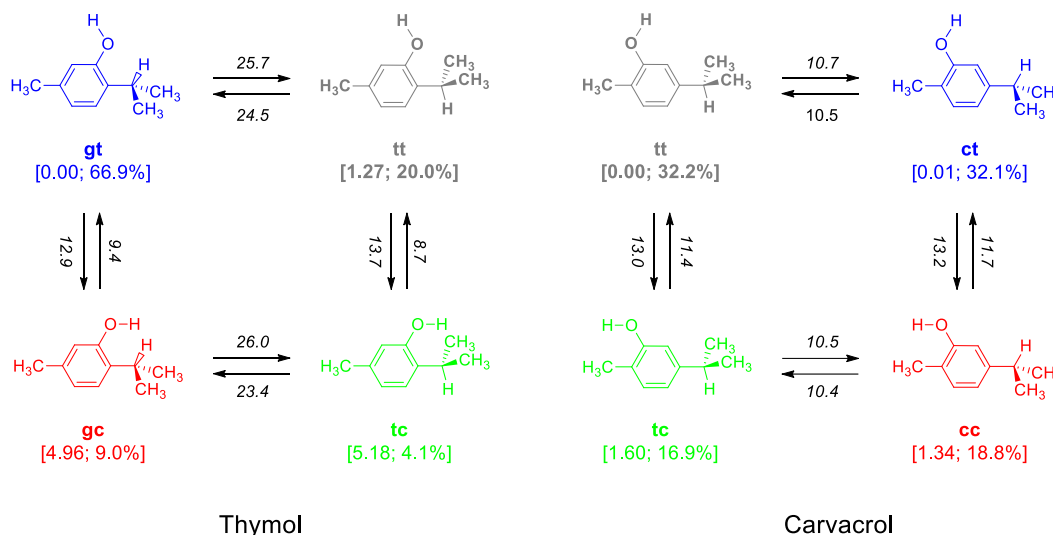


Figure 3. Conformers of thymol (2-isopropyl-5-methylphenol) and carvacrol (5-isopropyl-2-methylphenol), along with their B3LYP/6-311++G(d,p) Gibbs free energies at 298.15 K relative to the most stable conformer and corresponding Boltzmann populations (values in squared brackets). Energy barriers (including zero-point-vibrational energy correction) for the conformational interconversions are indicated next to the arrows representing these processes. All energies are expressed in kJ mol^{-1} . Conformers are labeled using two letters [**g** (\pm gauche), **t** (trans), or **c** (cis)] where the first letter denotes the orientation of the isopropyl group and the second refers to the orientation of the hydroxyl group relative to the nearest alkyl fragment, as detailed in the text.

3.2. Mid- and Near-IR Spectra of Thymol and Carvacrol Isolated in Solid N_2 at 15 K

The experimental mid-IR spectra ($1550\text{--}745\text{ cm}^{-1}$) of thymol and carvacrol, recorded immediately after their deposition in a low-temperature N_2 matrix, are shown in **Figures 4a** and **5a**, respectively. These spectra are slightly different from those recorded in noble gas matrices (see **Figures S1** and **S2** in the supplementary material for further details), with minor deviations in band positions, particularly in the OH stretching region, which is highly sensitive to matrix effects, and in the relative intensities of certain bands. To aid in the interpretation of the experimental spectra, harmonic vibrational calculations were performed at the B3LYP/6-311++G(d,p) level for the conformers predicted to be present in the matrices.

For thymol, the experimental spectrum of the freshly deposited N_2 matrix at 15 K (**Figure 4a**) is very well reproduced by the theoretical spectrum simulated from a mixture of the **gt** and **tt** conformers (**Figure 4b**). This spectrum was simulated from the vibrational data computed for both conformers, with the relative intensities of **gt** and **tt** scaled by 1.0 and 0.15, respectively, to achieve a good agreement with the experimental data. Although the calculated stick IR spectra of the two



conformers are overall quite similar (**Figure 4c**), some bands in the 1300–1000 cm^{-1} region can be unambiguously assigned to the dominant **gt** conformer (see **Figure S3** for details). These include the features at 1295, 1278, 1218, 1166, 1154, 1117, 1090, and 1065 cm^{-1} . In contrast, the experimental identification of the **tt** conformer is considerably more challenging, since most of its IR features overlap with those of the most abundant **gt** conformer. Nevertheless, subtle shoulders at 1286, 1229 and 1127 cm^{-1} , as well as the weak band at 1051 cm^{-1} , can be tentatively attributed to the **tt** form (**Figure S3**). Notably, its strongest absorption predicted at 1123 cm^{-1} ($A^{\text{th}} = 111.8 \text{ km mol}^{-1}$) has a very weak experimental counterpart at 1127 cm^{-1} . This provides further evidence for the significantly lower abundance of the **tt** form in the deposited N_2 matrix as compared with the **gt** conformer, in line with the theoretical predictions.

Regarding carvacrol, the spectroscopic identification of individual conformers in the deposited N_2 matrix (**Figure 5a**), by comparison with the calculated spectra (**Figures 5b** and **5c**), proves even more challenging than in the case of thymol. This difficulty arises because all four conformers have appreciable gas-phase populations and display very similar spectral profiles. The only reliable markers are the doublets observed at 1527/1507 cm^{-1} and 1117/1104 cm^{-1} . In the first case, the higher-frequency component can be attributed to the two most stable conformers **tt** and **ct**, whereas the lower-frequency one corresponds to the higher-energy forms **tc** and **cc**. The second doublet occurs in a spectral region where only the two lower-energy conformers absorb, and their predicted bands do not overlap. Thus, the higher- and lower-frequency components of this doublet can be assigned to the **tt** and **ct** conformers, respectively.

In summary, the spectral analysis of matrix isolated thymol and carvacrol confirms the presence of the most stable trans-OH conformers in the matrix and, due to the stabilizing effect of the N_2 matrix as compared to the noble gas matrices, suggests the possible presence of the high-energy cis-OH conformers in carvacrol. However, the strong spectral overlap prevents an unambiguous identification of the conformers. This limitation underscores the importance of complementary techniques, such as selective NIR vibrational excitation, to manipulate and probe conformational populations. The results of these NIR irradiation experiments are presented in section 3.3 and based on these results comprehensive spectral assignments are provided in **Tables S1-S4**.



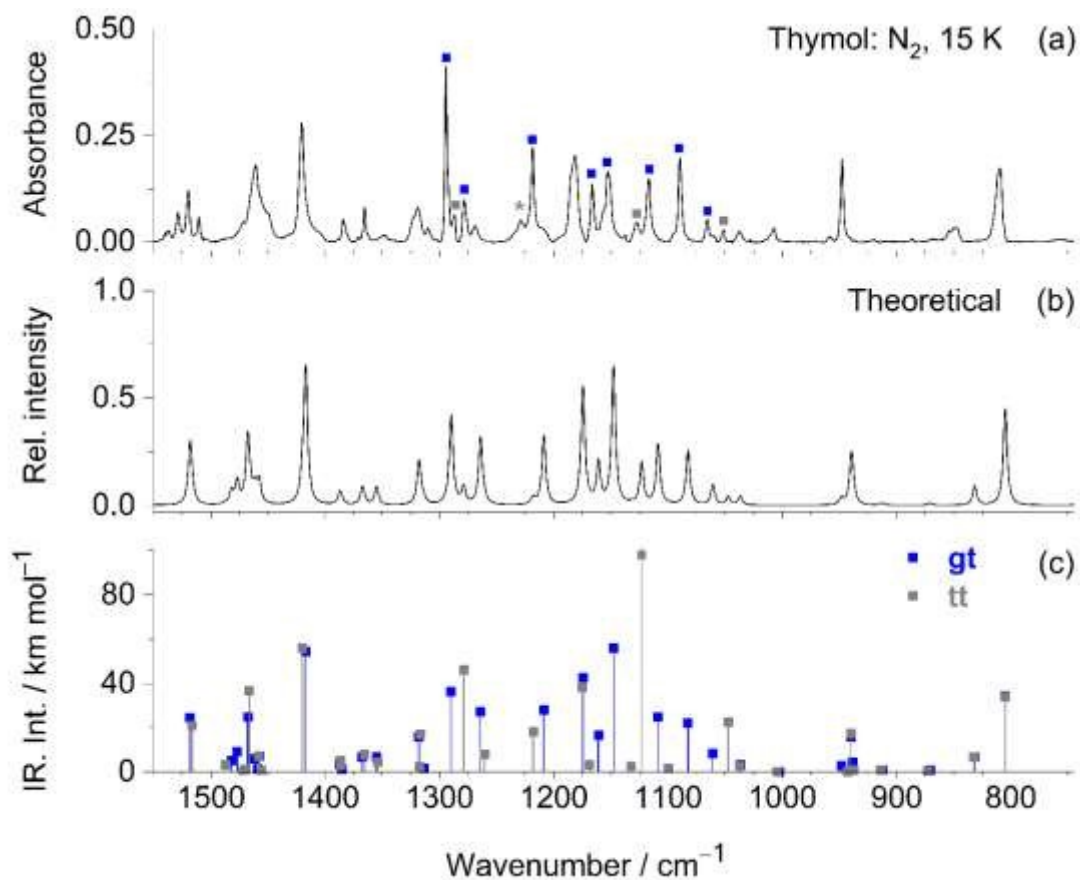


Figure 4. (a) Experimental mid-IR spectrum of thymol recorded after isolating monomers of the compound in a N₂ matrix at 15 K. (b) Theoretical spectrum of a mixture of the **gt** and **tt** conformers, which was simulated from the B3LYP/6-311++G(d,p) vibrational calculations carried out for both conformers. Bands highlighted with blue and grey squares are assigned to the **gt** and **tt** conformers, respectively, by comparison with the computed vibrational data. The band at 1229 cm⁻¹, marked with an asterisk, is tentatively attributed to the **tt** conformer, but it may also originate from the high-energy **cc** conformer, as demonstrated by the results of the NIR irradiation experiments discussed in Section 3.3. Lorentzian functions (FWHM = 4 cm⁻¹) centered at the calculated wavenumbers were used and the intensities were scaled by 1.0 (**gt**) and 0.15 (**tt**) to best match the experimental spectrum. (c) Scaled wavenumbers and unscaled IR intensities extracted from the harmonic vibrational calculations performed for the **gt** (blue squares) and **tt** (grey squares) conformers.



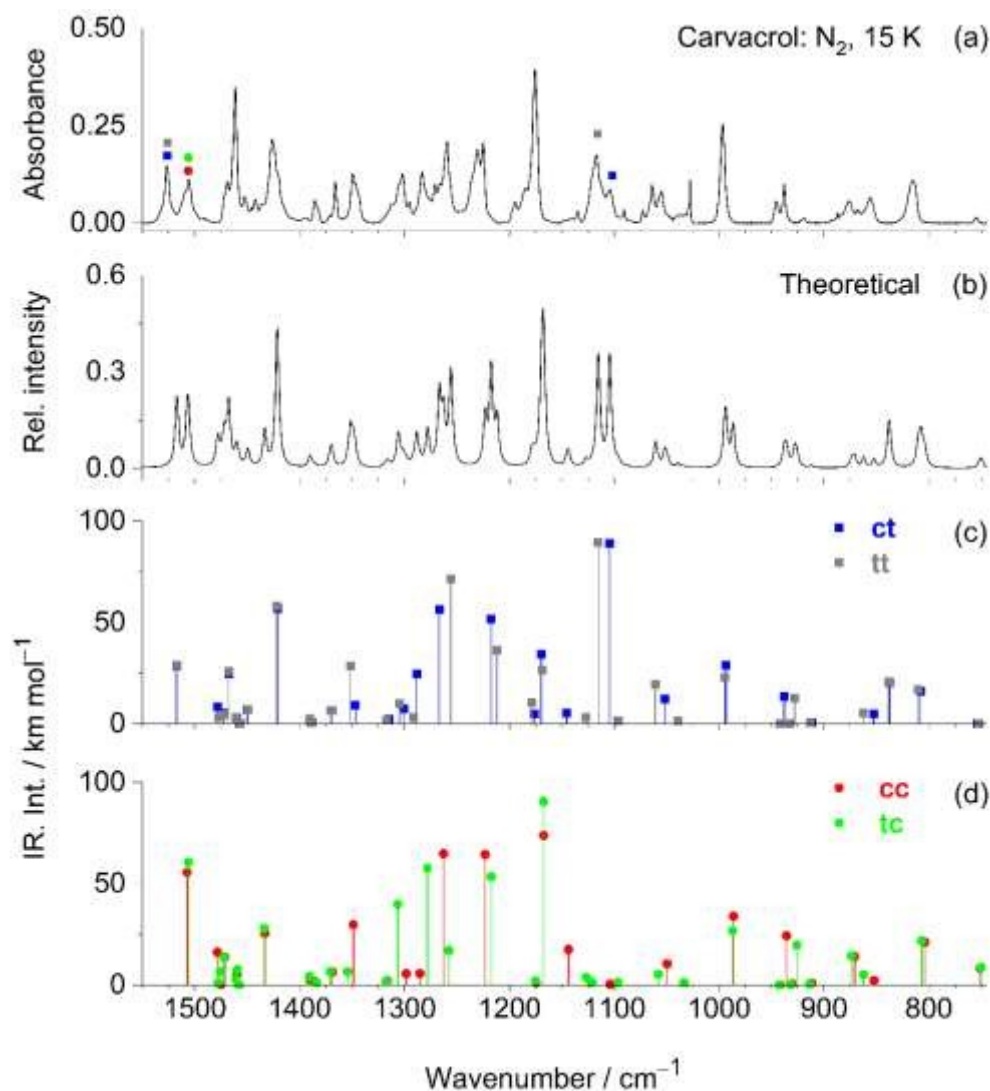


Figure 5. (a) Experimental mid-IR spectrum of carvacrol recorded after isolating monomers of the compound in a N_2 matrix at 15 K. (b) Theoretical spectrum of a mixture of the **tt**, **ct**, **tc** and **cc** conformers, which was simulated from the B3LYP/6-311++G(d,p) vibrational calculations carried out for each species. Lorentzian functions (FWHM = 4 cm^{-1}) centered at the calculated wavenumbers were used and the intensities were scaled by 1:1:0.5:0.6 to best match the experimental spectrum. (c,d) Scaled wavenumbers and unscaled IR intensities extracted from the harmonic vibrational calculations performed for the **ct** (blue squares), **tt** (grey squares), **cc** (red circles) conformers. **tc** (green circles).

The IR spectra of thymol and carvacrol isolated in solid N_2 were also recorded in the near-IR region ($7500\text{--}4000\text{ cm}^{-1}$) to determine the positions of the OH-stretching overtone ($2\nu_{OH}$) bands, which are required for selecting the wavenumbers for NIR irradiations. In both compounds, the $2\nu_{OH}$ absorption appears as a broad band from 7110 to 7060 cm^{-1} , centered at $\sim 7082\text{ cm}^{-1}$ (**Figures 6c** and **6d**), which mirrors the ν_{OH} band profile centered at $\sim 3625\text{ cm}^{-1}$ (**Figures 6e** and



6f). Anharmonic frequency calculations at the B3LYP/6-311++G(2d,2p) are in good agreement with the experimental data. For thymol, 2 ν_{OH} transitions are predicted at 7128 and 7145 cm^{-1} for the **gt** and **tt** conformers, respectively, while for carvacrol, the four conformers overlap more strongly, with 2 ν_{OH} transitions between 7129 and 7132 cm^{-1} .

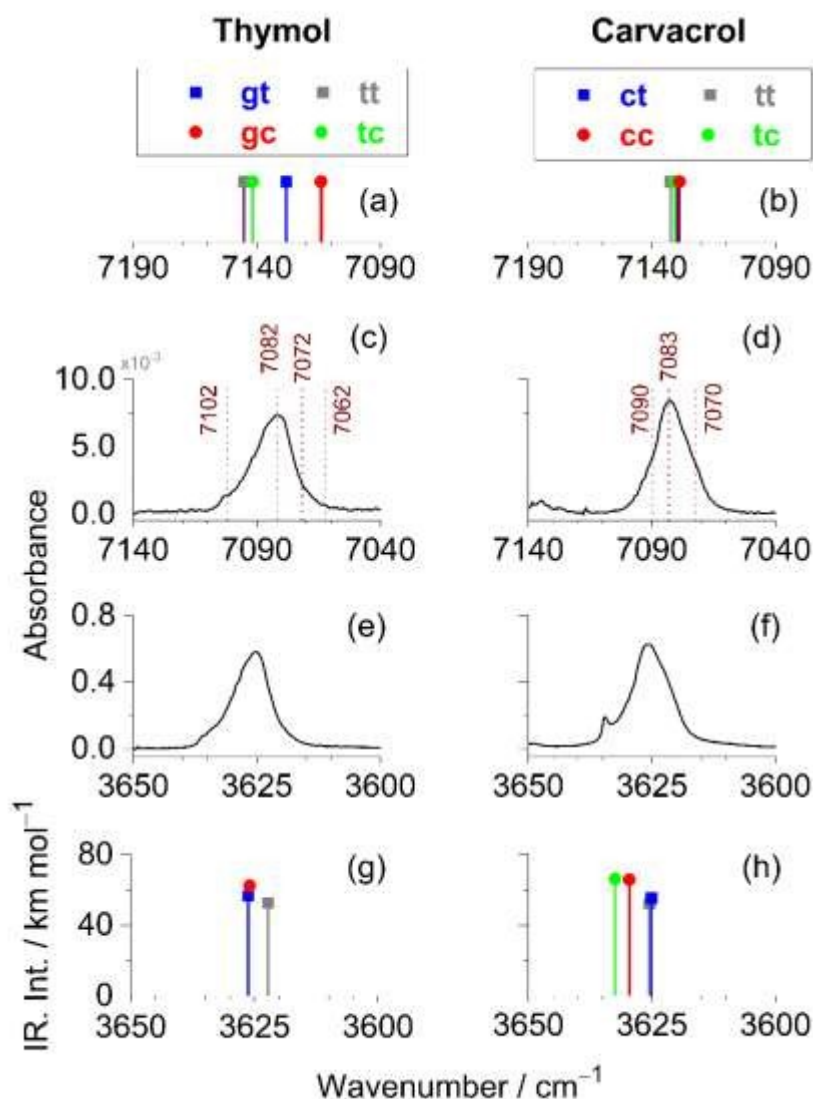


Figure 6. Fragments of the near-IR (c,d) and mid-IR (e,f) spectra of thymol and carvacrol isolated in solid N_2 at 15 K showing the 2 ν_{OH} and ν_{OH} absorption bands, respectively. The dotted vertical lines in panels (c) and (d) indicate the wavenumbers applied in the narrowband NIR irradiations of the matrix isolated compounds. The 2 ν_{OH} and ν_{OH} absorption bands are compared with results of anharmonic (a,b) and harmonic (g,h) vibrational calculations carried out at the B3LYP/6-311++G(2d,2p) and B3LYP/6-311++G(d,p) levels of theory, respectively, for the conformers of both molecules. The ν_{OH} mode computed for the **tc** conformer of thymol (3652.3 cm^{-1} ; $A^{\text{th}} = 83.9 \text{ km mol}^{-1}$) is not shown as it is predicted outside of the spectral range shown. Anharmonic wavenumbers are unscaled while the harmonic ones were scaled by 0.945.



3.3. Conformational Conversions Induced by NIR laser-Light Irradiations

Due to the relatively broad profile of the $2\nu_{\text{OH}}$ overtone bands, in the irradiation experiments, narrowband NIR light was tuned not only at the wavenumber corresponding to the band center but also at wavenumbers slightly offset to the higher- and lower-frequency sides. This approach ensured that the laser beam, with its narrower bandwidth compared to the overtone band, effectively targeted multiple spectral positions within the $2\nu_{\text{OH}}$ absorption profile to maximize selectivity. The changes triggered by the NIR irradiations were monitored by collecting mid-IR spectra.

3.3.1. Thymol

The first set of irradiation experiments was performed by tuning the laser to 7102 cm^{-1} , followed by 7082 cm^{-1} , corresponding respectively to the high-frequency side and the center of the $2\nu_{\text{OH}}$ band. Exposing matrix-isolated thymol to NIR radiation at these wavenumbers for approximately 20 minutes each resulted in similar spectral changes (more pronounced upon irradiation at the lower wavenumber), indicating the occurrence of conformational isomerization. These spectral changes are reflected in the difference IR spectrum shown in **Figure 7b**, obtained by subtracting the pre-irradiation spectrum from the post-irradiations' spectrum. As illustrated in this difference spectrum, these irradiations resulted in an increase in the intensity of a specific set of bands (highlighted with red circles) alongside a simultaneous decrease in the intensity of another set of bands (marked with blue squares). These observations provide clear evidence of NIR-induced conformational changes taking place in matrix-isolated thymol.

Subsequent irradiations were conducted on the lower-frequency side of the $2\nu_{\text{OH}}$ profile, specifically at 7072 and 7062 cm^{-1} . The results of these irradiations, as reflected in the difference spectrum shown in **Figure 7c**, reveal that the bands which had previously increased in intensity now displayed a clear decrease, while those that had decreased in intensity showed a corresponding increase. This reversal in the spectral behavior unequivocally demonstrates that excitation at 7072 and 7062 cm^{-1} induces the opposite conformational transformation(s) to those triggered by excitation at the 7102 and 7082 cm^{-1} .



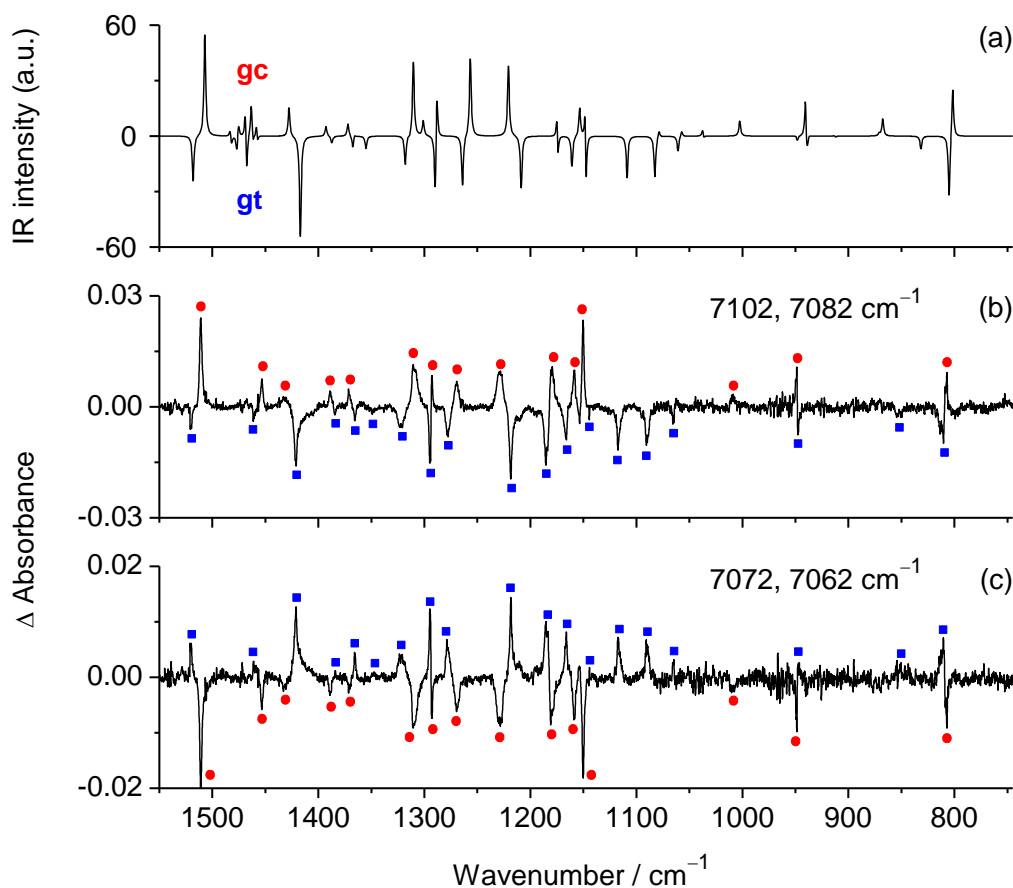


Figure 7. Spectral indication of conformational changes in thymol isolated in solid N₂ (15 K) following excitation of the 2νOH mode, supported by simulated IR spectra of the involved conformers. (b) Spectrum recorded after a total of 40 min of NIR irradiations at 7102 and 7082 cm⁻¹ (20 minutes each) minus that recorded before the irradiations (positive bands indicate conformer formation upon irradiation). (c) Spectrum recorded after a total of 40 min of NIR irradiations at 7072 and 7062 cm⁻¹ (20 minutes each) minus that recorded before these irradiations (positive bands indicate conformer formation upon the irradiations). (a) B3LYP/6-311++G(d,p) simulated IR difference spectrum for the conversion of conformer **gt** to **gc** (intensity ratio 1:1).

To support the assignment of the conformers being consumed or produced during the NIR irradiations, the experimental difference spectra were compared with the B3LYP/6-311++G(d,p) theoretical spectra of all four thymol conformers. This analysis revealed that the spectral changes induced by NIR irradiation are well reproduced by the theoretical difference spectrum **gc minus gt**, shown in **Figure 7a**. Accordingly, irradiations at 7102 and 7082 cm⁻¹ promote the **gt** → **gc** conversion, while irradiations at 7072 and 7062 cm⁻¹ induce the reverse **gc** → **gt** transition, in agreement with the anharmonic vibrational calculations which predict the 2νOH overtone of **gt** conformer at a higher frequency than that of **gc**. This bidirectional behavior provides evidence of



the reversible nature of the NIR-induced conformational interconversion, as illustrated in **Figure 8**. The spectral signatures of the **gt** and **gc** conformers, extracted from the experimental difference spectra shown in **Figure 7**, are listed in **Tables S1** and **S2**, respectively. These tables also include approximate assignments of the corresponding vibration modes.

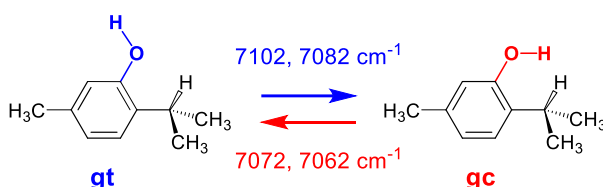


Figure 8. Bidirectional NIR-induced OH-rotamerization observed for thymol isolated in a low temperature N₂ matrix.

It is important to note that no spectral evidence of interconversion between the **gt** and **tt** conformers was detected upon excitation of the $2\nu_{\text{OH}}$ mode, consistent with our previous results in a Xe matrix⁵⁵. This confirms that isopropyl rotamerization does not occur under these conditions, suggesting that energy redistribution within the molecule preferentially channels into the OH-rotamerization rather than facilitating the isopropyl group rotation.

Furthermore, no spectral indication of interconversion between the **tt** and **tc** conformers were observed. This conclusion is supported by a detailed analysis of the spectral changes in the 1300-1000 cm⁻¹ region where, as mentioned above, conformer **tt** shows weak absorptions at 1286, 1129 and 1051 cm⁻¹. Notably, these three bands remain unaffected by NIR irradiations at 7102 and 7082 cm⁻¹ (see Figure S4 for details). One possible explanation is that the **tt** conformer is not effectively excited during the laser irradiation; however, this is unlikely given that the entire $2\nu_{\text{OH}}$ band profile was scanned. A more plausible hypothesis is that **tt** is indeed converted to **tc** upon NIR excitation, but the latter rapidly relaxes back to **tt** via H-atom tunneling, which prevents any observable net change in the **tt** population under steady-state conditions. This interpretation is consistent with the tunneling decay results, which will be presented and discussed in Section 3.4.



3.3.2. Carvacrol

Irradiation experiments were also carried out on carvacrol isolated in an N₂ matrix. The sample was exposed to the OPO tunable narrowband light at 7090, 7083, and 7072 cm⁻¹, corresponding to the low-frequency edge, maximum, and high-frequency edge of the 2ν_{OH} absorption band, respectively, for about 20 minutes each. Mid-IR spectra were recorded after each irradiation, and the resulting spectral changes are presented in **Figure 9**.

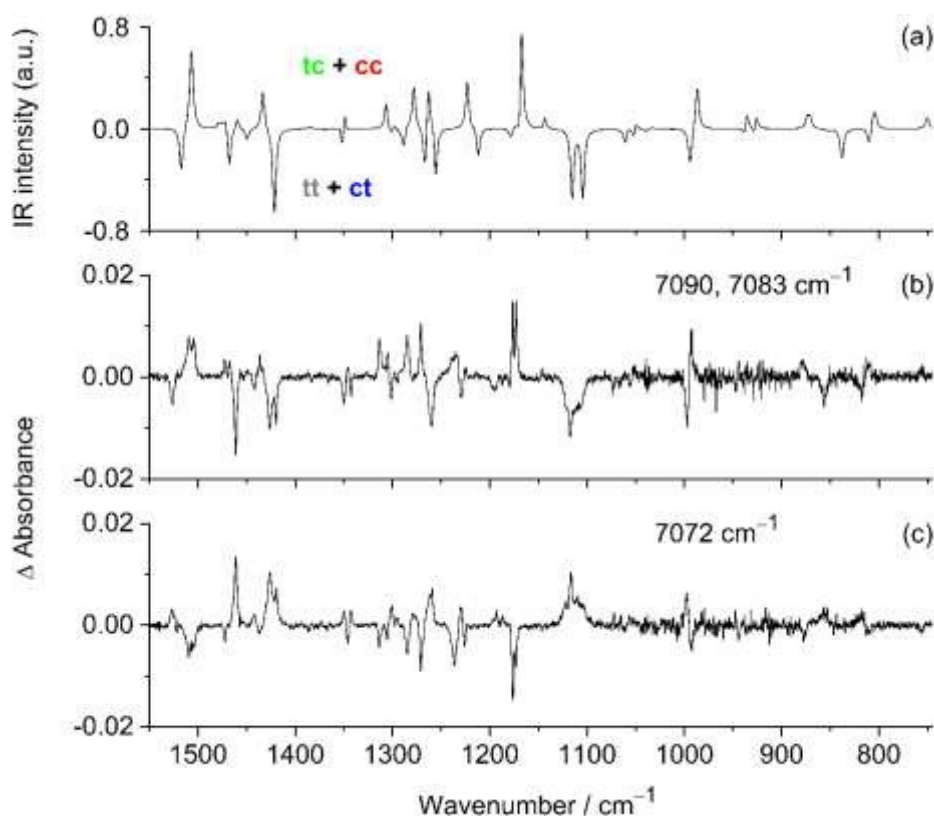


Figure 9. Spectral indication of conformational changes in carvacrol isolated in solid N₂ (15 K) following excitation of the 2ν_{OH} mode, supported by simulated IR spectra of the involved conformers. (b) Spectrum recorded after a total of 20 min of NIR irradiations at 7090 or 7083 cm⁻¹ minus that recorded before these irradiations (positive bands indicate conformer formation upon irradiation). (c) Spectrum recorded after a total of 20 min of NIR irradiations at 7072 cm⁻¹ minus that recorded before these irradiations (positive bands indicate conformer formation upon the irradiations). (a) B3LYP/6-311++G(d,p) simulated IR difference spectrum for the conversion of conformers **tt + ct** into conformers **tc + cc** (intensity ratio 1:1).

Comparison of the theoretical and experimental difference spectra clearly shows the occurrence of the **tt** → **tc** and **ct** → **cc** isomerizations upon irradiation at 7090 or 7083 cm⁻¹, whereas the reverse transformations are promoted by irradiation at 7072 cm⁻¹ (**Figure 10**). These



spectral changes provide clear evidence for the presence of two sets of conformers in the N₂ matrix, namely **tt** + **ct** and **tc** + **cc**. When this result is considered together with the spectral indication of the presence of the **tt** and **ct** conformers in the as-deposited matrix (supported by the doublet at 1117/1104 cm⁻¹), and with the fact that several of the bands that increase upon the irradiations at 7090/7083 cm⁻¹ were already discernible in the pre-irradiation spectrum, taken together, the data strongly support the presence of all four conformers in the N₂ matrix, consistently with the theoretical predictions. Nevertheless, the conformer-by-conformer assignment remains less definitive than in the case of thymol. The assignment of the experimental spectra to the two conformer sets is provided in **Tables S3** and **S4**.

It is important to note that, as in the case of thymol, we were unable to identify spectral features associated with isopropyl group rotamerization, which would lead to interconversion between the **tt** and **ct** conformers or between the **tc** and **cc** conformers. This result is particularly striking, as one might initially expect that excitation of the 2νOH overtone in carvacrol would induce isopropyl isomerization, given that its barrier is much lower than in thymol (by a factor of ~2.5) and is of the same order as that for the OH rotamerization (with the caveat that rotation of the bulky isopropyl group may be partially hindered in an N₂ matrix). The most plausible explanation is that the initially excited state, namely the OH-stretching overtone, couples more efficiently, via anharmonic IVR, to motions involving the hydroxyl group, in particular to the OH torsional coordinate. The behaviour of carvacrol is therefore consistent with a mode-selective process, whereby excitation of the 2νOH overtone preferentially drives OH-rotamerization:



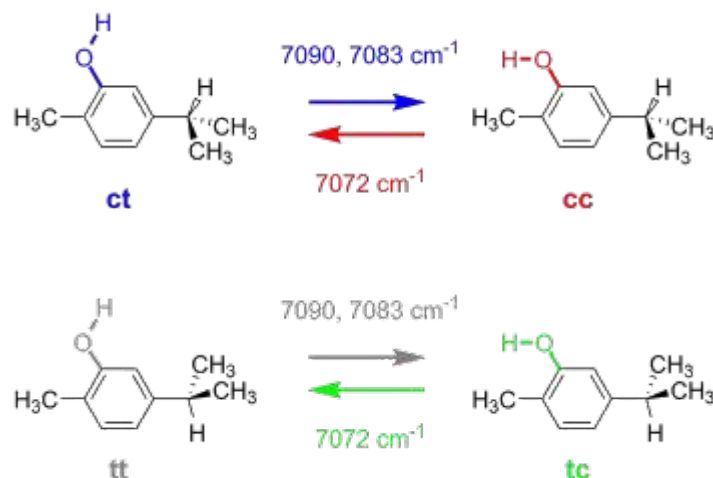


Figure 10. Bidirectional NIR-induced OH-rotamerization observed for carvacrol isolated in a low-temperature N₂ matrix.

3.4. Decay of the Higher-Energy cis-OH Conformers Under Dark Conditions

Once the high-energy conformers were generated by selective excitation of the 2νOH overtones of their low-energy counterparts (7102 and 7082 cm⁻¹ for thymol, and 7090 and 7083 cm⁻¹ for carvacrol), the sample was maintained under dark conditions for approximately one hour. During this period, a limited number of IR spectra were collected using a 2200 cm⁻¹ cutoff filter and restricting each acquisition to 32 scans, thereby minimizing exposure to residual spectrometer radiation and preventing any unwanted photoinduced processes. The spectral changes observed under these conditions, shown in **Figure 11**, provide unambiguous evidence that the higher-energy cis-OH conformers (**gc** in thymol; **tc** and **cc** in carvacrol) decay into their lower-energy trans-OH counterparts (**gt** in thymol; **tt** and **ct** in carvacrol) by means of H-atom tunneling.



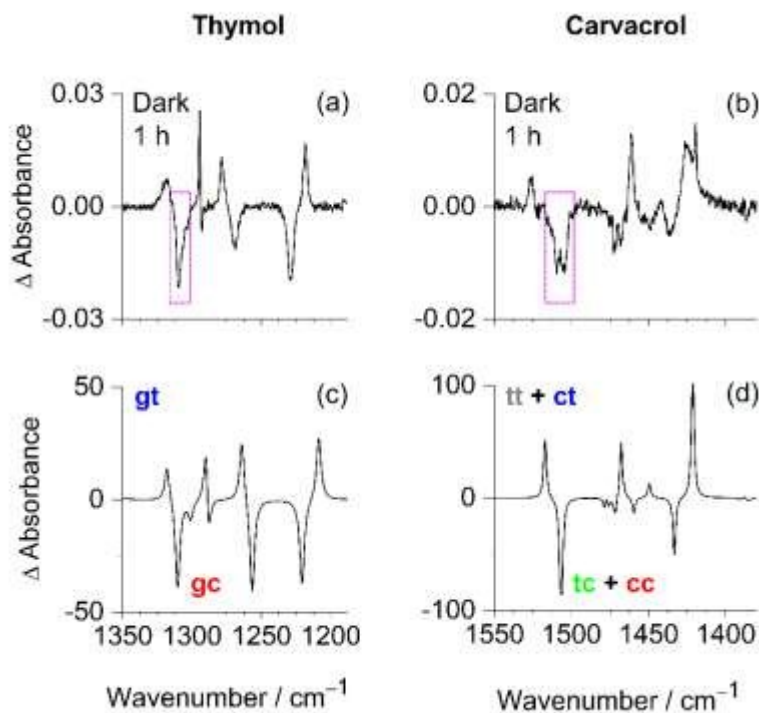


Figure 11. (a,b) Fragments of experimental difference spectra showing the spectral changes observed after keeping matrix-isolated thymol and carvacrol (N_2 , 15 K) in dark for 1 hour. Prior to the dark period, the samples were enriched in the higher-energy cis-OH conformers by NIR laser irradiations at 7083–7082 cm^{-1} . The negative bands enclosed by a dotted rectangle were used to monitor the kinetics of the dark process. (c,d) B3LYP/6-311++G(d,p) theoretical difference spectra illustrating the conversion of the higher-energy cis-OH conformers into the lower-energy trans-OH conformers.

To quantitatively monitor the kinetics of the OH-rotamerization tunneling, specific diagnostic bands were selected: the band at 1310 cm^{-1} for thymol, which is assigned to the gc conformer (see Table S2), and the band at 1507 cm^{-1} for carvacrol, attributed to the tc and cc conformers (see Table S4). The time-dependent changes of the integrated absorbances (A) of the selected bands were fitted to a first-order kinetic model, $[A](t)/[A]_0 = e^{-kt}$, where $[A](t)$ and $[A]_0$ represent the absorbance of the diagnostic band at time t and initially, respectively, and from these fits the tunneling rate constants were estimated (**Figure 12**). For thymol, a tunneling rate constant of $(8.4 \pm 0.4) \times 10^{-4} s^{-1}$ was determined, corresponding to a half-life of ~ 14 minutes. In the case of carvacrol, a tunneling rate constant of $(5.4 \pm 0.3) \times 10^{-4} s^{-1}$ was obtained, corresponding to a half-life of ~ 21 minutes. The rapid conversion of the high-energy cis-OH rotamers into the more stable trans-OH forms indicates that the cis-OH \rightarrow trans-OH isomerization previously observed under NIR irradiation is also driven by an H-tunneling mechanism.



The estimated values are comparable to OH-rotamerization tunneling rates reported for other phenol derivatives under similar experimental conditions, such as 2-cyanophenol²⁸ and 2-isocyanophenol²⁹. The slightly slower OH-rotamerization tunneling rate observed for carvacrol in relation to thymol is consistent with the qualitative trend in the calculated cis-OH \rightarrow trans-OH barriers shown in Figure 3 (11-12 kJ mol⁻¹ for **cc** \rightarrow **ct** and **tc** \rightarrow **tt** in carvacrol compared to 9 kJ mol⁻¹ for **gc** \rightarrow **gt** in thymol, **Figure 3**).

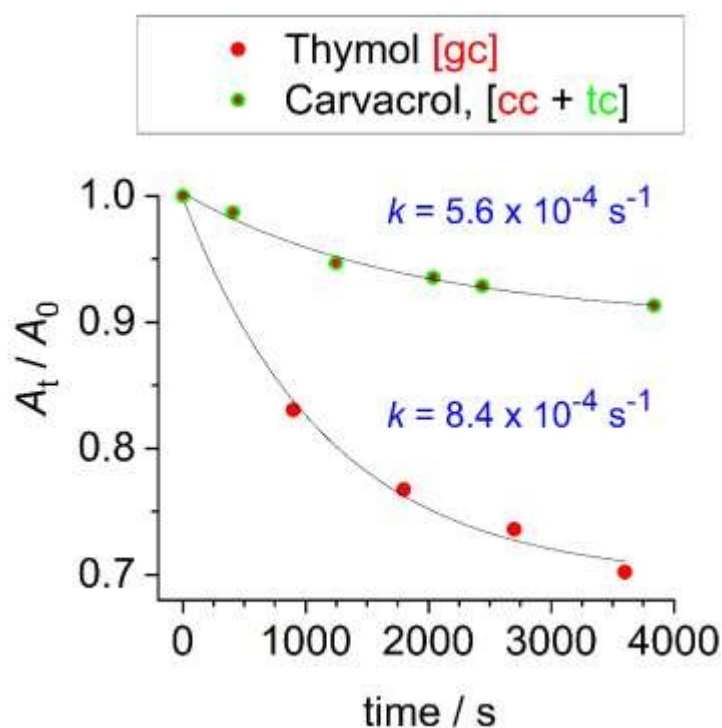


Figure 12. Time evolution of the high-energy **gc** conformer of thymol (red circles in the lower curve) and of the high-energy **cc** and **tc** conformers of carvacrol (green circles with red-filled centers in the upper curve) under dark conditions. The decay was monitored by integrating the vibrational bands at 1310 cm⁻¹ (thymol) and 1507 cm⁻¹ (carvacrol). Absorbances measured after 15 h in the dark, when no further spectral changes occurred, were subtracted from the time-dependent values to correct for the non-reactive conformers (70% for thymol and 90% for carvacrol). The corrected absorbances (A_t) were normalized to the initial absorbances (A_0) to obtain the relative populations of the reactive conformers. Solid lines represent the best single-exponential fits to the experimental data for carvacrol and thymol, respectively ($R^2 = 0.99$).

In our previous study on thymol, we have computed the tunneling probabilities for the **gc** \rightarrow **gt** and **tc** \rightarrow **tt** conversions in gas phase, and from these values, the corresponding tunneling rates and half-lives were derived. It was found that the half-life time of the **gc** \rightarrow **gt** process is



approximately 12.5 times longer than that of the **tc** → **tt** process, reflecting a more efficient tunneling pathway in the latter case. Assuming that a similar ratio holds under N₂ matrix isolation conditions, the expected half-life for the **tc** → **tt** conversion would be on the order of ~1 minute. This rapid decay provides a consistent explanation for the experimental observation reported above that the bands attributed to the **tt** conformer remain essentially unaffected by the NIR irradiations. In fact, if the **tc** conformer is photogenerated under these conditions, it would promptly relax back to **tt** on a timescale too short to be spectroscopically detected.

4. Concluding Discussion

Carvacrol and thymol were isolated in an N₂ cryogenic matrix at 15 K. Spectroscopic analysis provided evidence for the presence of the lower-energy trans-OH conformers (**gt** and **tt** in thymol; **tt** and **ct** in carvacrol) in the as-deposited matrix for both molecules. Higher-energy cis-OH conformers were observed only for carvacrol (**tc** and **cc**).

Excitation of the 2νOH overtones of the trans-OH conformers with NIR laser light induced the **gt** → **gc** process in thymol and the **tt** → **tc** and **ct** → **cc** processes in carvacrol. These findings demonstrate that the energy absorbed in the first OH-stretch overtone is efficiently channeled into the torsional coordinate, driving rotamerization of the same hydroxyl group. Furthermore, these OH-induced interconversions could be selectively reversed by fine-tuning the irradiation frequency. No evidence of isopropyl group rotamerization was detected in either compound. While this outcome was somehow expected for thymol given that the energy barrier for isopropyl rotation is significantly higher than that for OH-rotamerization, it is unexpected in the case of carvacrol, where the isopropyl rotational barrier is lower than in thymol and comparable to the OH-rotamerization barrier. These results demonstrate that regardless of the magnitude of the energy barriers for the internal rotation of the hydroxyl and isopropyl groups, IVR preferentially couples the excited 2νOH mode to the local OH-rotamerization coordinate rather than the C₃H₇-rotamerization coordinate.

Finally, the kinetic measurements performed in dark provided unambiguous evidence that the high-energy cis-OH revert to their more stable trans-OH forms through OH-rotamerization tunneling. The estimated tunneling rate constants were approximately 8×10^{-4} and $5 \times 10^{-4} \text{ s}^{-1}$, for thymol and carvacrol, respectively, corresponding to half-life times of about 14–21 minutes, values



consistent with those reported for related phenolic systems. From the experimental results obtained for thymol and previous tunneling calculations performed for this molecule in vacuum, which predicted that the **tc** → **tt** process proceeds roughly 12.5 times faster than the **gc** → **gt** one, the half-life of the **tc** → **tt** conversion in the N₂ matrix can be estimated to be approximately one minute. This likely accounts for the apparent stability of the **tt** conformer during NIR irradiation, as any transient **tc** population would decay too rapidly to be detected experimentally.

Acknowledgments

L.J.D. (postdoctoral fellowship #2022/09269-1) and A.A.C.B. (grant #2015/01491-3) are grateful to the São Paulo Research Foundation (FAPESP) for financial support. A.A.C.B. also thanks the Conselho Nacional de Desenvolvimento Científico e Tecnológico (CNPq) of Brazil for academic support (Grant #313720/2023-1). R.F. thanks the Horizon-Widerra-2023-Talents-01 ERA-Chair 1011848998 Spectroscopy@IKU “*Manipulating and Characterizing Molecular Architectures: From Isolated Molecules to Molecular Crystals*” (Funded by the European Union) for financial support. The authors acknowledge the Coimbra Chemistry Centre – Institute of Molecular Sciences (CQC-IMS) which is supported by the Fundação para a Ciência e a Tecnologia (FCT), Portuguese Agency for Scientific Research. CQC is funded by FCT through projects UID/PRR/00313/2025 (<https://doi.org/10.54499/UID/PRR/00313/2025>) and UID/00313/2025 (<https://doi.org/10.54499/UID/00313/2025>) and IMS through special complementary funds provided by FCT (project LA/P/0056/2020 <https://doi.org/10.54499/LA/P/0056/2020>). The authors also acknowledge the Laboratory for Advanced Computing at University of Coimbra (UC-LCA) for providing computing resources that have contributed to the research results reported within this paper, and Coimbra Laser Lab (CLL) for providing experimental facilities.

References

- (1) Pettersson, M.; Lundell, J.; Khriachtchev, L.; Räsänen, M. IR Spectrum of the Other Rotamer of Formic Acid, *Cis* -HCOOH. *J. Am. Chem. Soc.* **1997**, *119* (48), 11715–11716. <https://doi.org/10.1021/ja972362l>.
- (2) Pettersson, M.; Maçôas, E. M. S.; Khriachtchev, L.; Lundell, J.; Fausto, R.; Räsänen, M. *Cis* → *Trans* Conversion of Formic Acid by Dissipative Tunneling in Solid Rare Gases: Influence of Environment on the Tunneling Rate. *J. Chem. Phys.* **2002**, *117* (20), 9095–9098. <https://doi.org/10.1063/1.1521429>.



- (3) Maçôas, E. M. S.; Khriachtchev, L.; Pettersson, M.; Fausto, R.; Räsänen, M. Rotational Isomerism in Acetic Acid: The First Experimental Observation of the High-Energy Conformer. *J. Am. Chem. Soc.* **2003**, *125* (52), 16188–16189. <https://doi.org/10.1021/ja038341a>.
- (4) Maçôas, E. M. S.; Khriachtchev, L.; Pettersson, M.; Fausto, R.; Räsänen, M. Internal Rotation in Propionic Acid: Near-Infrared-Induced Isomerization in Solid Argon. *J. Phys. Chem. A* **2005**, *109* (16), 3617–3625. <https://doi.org/10.1021/jp044070u>.
- (5) Maçôas, E. M. S.; Khriachtchev, L.; Pettersson, M.; Fausto, R.; Räsänen, M. Rotational Isomerization of Small Carboxylic Acids Isolated in Argon Matrices: Tunnelling and Quantum Yields for the Photoinduced Processes. *Phys Chem Chem Phys* **2005**, *7* (5), 743–749. <https://doi.org/10.1039/B416641H>.
- (6) Reva, I.; Nunes, C. M.; Biczysko, M.; Fausto, R. Conformational Switching in Pyruvic Acid Isolated in Ar and N₂ Matrixes: Spectroscopic Analysis, Anharmonic Simulation, and Tunneling. *J. Phys. Chem. A* **2015**, *119* (11), 2614–2627. <https://doi.org/10.1021/jp509578c>.
- (7) Kuş, N.; Fausto, R. Effects of the Matrix and Intramolecular Interactions on the Stability of the Higher-Energy Conformers of 2-Fluorobenzoic Acid. *J. Chem. Phys.* **2017**, *146* (12), 124305. <https://doi.org/10.1063/1.4978794>.
- (8) Halasa, A.; Lapinski, L.; Reva, I.; Rostkowska, H.; Fausto, R.; Nowak, M. J. Near-Infrared Laser-Induced Generation of Three Rare Conformers of Glycolic Acid. *J. Phys. Chem. A* **2014**, *118* (30), 5626–5635. <https://doi.org/10.1021/jp5051589>.
- (9) Halasa, A.; Lapinski, L.; Rostkowska, H.; Reva, I.; Nowak, M. J. Tunable Diode Lasers as a Tool for Conformational Control: The Case of Matrix-Isolated Oxamic Acid. *J. Phys. Chem. A* **2015**, *119* (11), 2203–2210. <https://doi.org/10.1021/jp501448m>.
- (10) Apóstolo, R. F. G.; Bazsó, G.; Bento, R. R. F.; Tarczay, G.; Fausto, R. The First Experimental Observation of the Higher-Energy *Trans* Conformer of Trifluoroacetic Acid. *J. Mol. Struct.* **2016**, *1125*, 288–295. <https://doi.org/10.1016/j.molstruc.2016.06.077>.
- (11) Apóstolo, R. F. G.; Bazsó, G.; Ogruc-Ildiz, G.; Tarczay, G.; Fausto, R. Near-Infrared *in Situ* Generation of the Higher-Energy *Trans* Conformer of Tribromoacetic Acid: Observation of a Large-Scale Matrix-Site Changing Mediated by Conformational Conversion. *J. Chem. Phys.* **2018**, *148* (4), 044303. <https://doi.org/10.1063/1.5010288>.
- (12) Bazsó, G.; Góbi, S.; Tarczay, G. Near-Infrared Radiation Induced Conformational Change and Hydrogen Atom Tunneling of 2-Chloropropionic Acid in Low-Temperature Ar Matrix. *J. Phys. Chem. A* **2012**, *116* (20), 4823–4832. <https://doi.org/10.1021/jp212597y>.



- (13) Araujo-Andrade, C.; Reva, I.; Fausto, R. Tetrazole Acetic Acid: Tautomers, Conformers, and Isomerization. *J. Chem. Phys.* **2014**, *140* (6), 064306. <https://doi.org/10.1063/1.4864119>.
- (14) Wagner, J. P.; Reisenauer, H. P.; Hirvonen, V.; Wu, C.-H.; Tyberg, J. L.; Allen, W. D.; Schreiner, P. R. Tunnelling in Carbonic Acid. *Chem. Commun.* **2016**, *52* (50), 7858–7861. <https://doi.org/10.1039/C6CC01756H>.
- (15) Maçôas, E. M. S.; Fausto, R.; Pettersson, M.; Khriachtchev, L.; Räsänen, M. Infrared-Induced Rotamerization of Oxalic Acid Monomer in Argon Matrix. *J. Phys. Chem. A* **2000**, *104* (30), 6956–6961. <https://doi.org/10.1021/jp000634s>.
- (16) Maçôas, E. M. S.; Fausto, R.; Lundell, J.; Pettersson, M.; Khriachtchev, L.; Räsänen, M. Conformational Analysis and Near-Infrared-Induced Rotamerization of Malonic Acid in an Argon Matrix. *J. Phys. Chem. A* **2000**, *104* (50), 11725–11732. <https://doi.org/10.1021/jp002853j>.
- (17) Maçôas, E. M. S.; Fausto, R.; Lundell, J.; Pettersson, M.; Khriachtchev, L.; Räsänen, M. A Matrix Isolation Spectroscopic and Quantum Chemical Study of Fumaric and Maleic Acid. *J. Phys. Chem. A* **2001**, *105* (15), 3922–3933. <https://doi.org/10.1021/jp003802p>.
- (18) Kovács, B.; Kuş, N.; Tarczay, G.; Fausto, R. Experimental Evidence of Long-Range Intramolecular Vibrational Energy Redistribution through Eight Covalent Bonds: NIR Irradiation Induced Conformational Transformation of *E*-Glutaconic Acid. *J. Phys. Chem. A* **2017**, *121* (18), 3392–3400. <https://doi.org/10.1021/acs.jpca.7b00615>.
- (19) Halasa, A.; Reva, I.; Lapinski, L.; Rostkowska, H.; Fausto, R.; Nowak, M. J. Conformers of Kojic Acid and Their Near-IR-Induced Conversions: Long-Range Intramolecular Vibrational Energy Transfer. *J. Phys. Chem. A* **2016**, *120* (17), 2647–2656. <https://doi.org/10.1021/acs.jpca.6b01275>.
- (20) Lapinski, L.; Reva, I.; Rostkowska, H.; Halasa, A.; Fausto, R.; Nowak, M. J. Conformational Transformation in Squaric Acid Induced by Near-IR Laser Light. *J. Phys. Chem. A* **2013**, *117* (25), 5251–5259. <https://doi.org/10.1021/jp402128g>.
- (21) Bazsó, G.; Magyarfalvi, G.; Tarczay, G. Near-Infrared Laser Induced Conformational Change and UV Laser Photolysis of Glycine in Low-Temperature Matrices: Observation of a Short-Lived Conformer. *J. Mol. Struct.* **2012**, *1025*, 33–42. <https://doi.org/10.1016/j.molstruc.2012.04.066>.
- (22) Bazsó, G.; Magyarfalvi, G.; Tarczay, G. Tunneling Lifetime of the *Ttc* /*Vlp* Conformer of Glycine in Low-Temperature Matrices. *J. Phys. Chem. A* **2012**, *116* (43), 10539–10547. <https://doi.org/10.1021/jp3076436>.
- (23) Nunes, C. M.; Lapinski, L.; Fausto, R.; Reva, I. Near-IR Laser Generation of a High-Energy Conformer of L-Alanine and the Mechanism of Its Decay in a Low-Temperature Nitrogen Matrix. *J. Chem. Phys.* **2013**, *138* (12), 125101. <https://doi.org/10.1063/1.4795823>.



- (24) Najbauer, E. E.; Bazăs, G.; Apóstolo, R.; Fausto, R.; Biczysko, M.; Barone, V.; Tarczay, G. Identification of Serine Conformers by Matrix-Isolation IR Spectroscopy Aided by Near-Infrared Laser-Induced Conformational Change, 2D Correlation Analysis, and Quantum Mechanical Anharmonic Computations. *J. Phys. Chem. B* **2015**, *119* (33), 10496–10510. <https://doi.org/10.1021/acs.jpcc.5b05768>.
- (25) Lapinski, L.; Nowak, M. J.; Reva, I.; Rostkowska, H.; Fausto, R. NIR-Laser-Induced Selective Rotamerization of Hydroxy Conformers of Cytosine. *Phys. Chem. Chem. Phys.* **2010**, *12* (33), 9615. <https://doi.org/10.1039/c0cp00177e>.
- (26) Halasa, A.; Lapinski, L.; Rostkowska, H.; Nowak, M. J. Intramolecular Vibrational Energy Redistribution in 2-Thiocytosine: SH Rotamerization Induced by Near-IR Selective Excitation of NH₂ Stretching Overtone. *J. Phys. Chem. A* **2015**, *119* (35), 9262–9271. <https://doi.org/10.1021/acs.jpca.5b06221>.
- (27) Lapinski, L.; Reva, I.; Rostkowska, H.; Fausto, R.; Nowak, M. J. Near-IR-Induced, UV-Induced, and Spontaneous Isomerizations in 5-Methylcytosine and 5-Fluorocytosine. *J. Phys. Chem. B* **2014**, *118* (11), 2831–2841. <https://doi.org/10.1021/jp411423c>.
- (28) Lopes Jesus, A. J.; Nunes, C. M.; Reva, I.; Pinto, S. M. V.; Fausto, R. Effects of Entangled IR Radiation and Tunneling on the Conformational Interconversion of 2-Cyanophenol. *J. Phys. Chem. A* **2019**, *123* (20), 4396–4405. <https://doi.org/10.1021/acs.jpca.9b01382>.
- (29) Lopes Jesus, A. J.; Reva, I.; Nunes, C. M.; Roque, J. P. L.; Pinto, S. M. V.; Fausto, R. Kinetically Unstable 2-Isocyanophenol Isolated in Cryogenic Matrices: Vibrational Excitation, Conformational Changes and Spontaneous Tunneling. *Chem. Phys. Lett.* **2020**, *747*, 137069. <https://doi.org/10.1016/j.cplett.2019.137069>.
- (30) Lopes Jesus, A. J.; Reva, I.; Araujo-Andrade, C.; Fausto, R. Conformational Switching by Vibrational Excitation of a Remote NH Bond. *J. Am. Chem. Soc.* **2015**, *137* (45), 14240–14243. <https://doi.org/10.1021/jacs.5b08588>.
- (31) Lopes Jesus, A. J.; Fausto, R.; Reva, I. Conformational Changes in 5-Methoxyindole: Effects of Thermal, Vibrational, and Electronic Excitations. *J. Phys. Chem. A* **2017**, *121* (18), 3372–3382. <https://doi.org/10.1021/acs.jpca.7b01713>.
- (32) Lopes Jesus, A. J.; Nunes, C.; Fausto, R.; Reva, I. Conformational Control over an Aldehyde Fragment by Selective Vibrational Excitation of Interchangeable Remote Antennas. *Chem. Commun.* **2018**, *54* (38), 4778–4781. <https://doi.org/10.1039/C8CC01052H>.
- (33) Sharma, A.; Reva, I.; Fausto, R. Conformational Switching Induced by Near-Infrared Laser Irradiation. *J. Am. Chem. Soc.* **2009**, *131* (25), 8752–8753. <https://doi.org/10.1021/ja903211f>.



- (34) Lapinski, L.; Reva, I.; Rostkowska, H.; Lopes Jesus, A. J.; Vieira Pinto, S. M.; Fausto, R.; Nowak, M. J. Conformational Isomerizations by Rotation around C–C or C–N Bonds: A Comparative Study on Matrix-Isolated Glycolamide and *N*-Hydroxyurea Excited with Near-IR Laser Light. *J. Phys. Chem. A* **2019**, *123* (17), 3831–3839. <https://doi.org/10.1021/acs.jpca.9b01992>.
- (35) Ryazantsev, S. V.; Feldman, V. I.; Khriachtchev, L. Conformational Switching of HOCO Radical: Selective Vibrational Excitation and Hydrogen-Atom Tunneling. *J. Am. Chem. Soc.* **2017**, *139* (28), 9551–9557. <https://doi.org/10.1021/jacs.7b02605>.
- (36) Góbi, S.; Reva, I.; Csonka, I. P.; M. Nunes, C.; Tarczay, G.; Fausto, R. Selective Conformational Control by Excitation of NH Imino Vibrational Antennas. *Phys. Chem. Chem. Phys.* **2019**, *21* (45), 24935–24949. <https://doi.org/10.1039/C9CP05370K>.
- (37) Fausto, R.; Gómez-Zavaglia, A. Light Induced Reactions in Cryogenic Matrices (Highlights 2011–2012)†. In *Photochemistry*; Albini, A., Fasani, E., Eds.; The Royal Society of Chemistry, 2013; Vol. 41, p 0. <https://doi.org/10.1039/9781849737722-00012>.
- (38) Fausto, R.; Borba, A.; Gómez-Zavaglia, A. Light Induced Reactions in Cryogenic Matrices (Highlights 2013–2014). In *Photochemistry: Volume 43*; Fasani, E., Albini, A., Eds.; The Royal Society of Chemistry, 2015; Vol. 43, p 0. <https://doi.org/10.1039/9781782622772-00020>.
- (39) Fausto, R.; Nikitin, T.; Brás, E. M. Light Induced Reactions in Cryogenic Matrices (Highlights 2017–2018). In *Photochemistry: Volume 47*; Albini, A., Protti, S., Eds.; The Royal Society of Chemistry, 2019; Vol. 47, p 0. <https://doi.org/10.1039/9781788016520-00028>.
- (40) Fausto, R.; Nikitin, T.; Brás, E. M. Light Induced Reactions in Cryogenic Matrices (2019–2020). In *Photochemistry: Volume 49*; Crespi, S., Protti, S., Eds.; The Royal Society of Chemistry, 2021; Vol. 49, p 0. <https://doi.org/10.1039/9781839165269-00053>.
- (41) Fausto, R.; Ildiz, G. O.; Nunes, C. M. IR-Induced and Tunneling Reactions in Cryogenic Matrices: The (Incomplete) Story of a Successful Endeavor. *Chem. Soc. Rev.* **2022**, *51* (7), 2853–2872. <https://doi.org/10.1039/D1CS01026C>.
- (42) Freindorf, M.; Kraka, E.; Cremer, D. A Comprehensive Analysis of Hydrogen Bond Interactions Based on Local Vibrational Modes. *Int. J. Quantum Chem.* **2012**, *112* (19), 3174–3187. <https://doi.org/10.1002/qua.24118>.
- (43) Akulin, V. M.; Karlov, N. V. Redistribution of the Vibrational Energy in the Course of Laser Excitation of High Vibrational Levels of Polyatomic Molecules. *Sov. J. Exp. Theor. Phys.* **1980**, *52*, 1063.
- (44) Bondybey, V. E. Relaxation and Vibrational Energy Redistribution Processes in Polyatomic Molecules. *Ann Rev Phys Chem* **1984**, *35*, 591–612. <https://doi.org/10.1146/annurev.pc.35.100184.003111>.



- (45) Felker, P. M.; Zewail, A. H. Dynamics of Intramolecular Vibrational-energy Redistribution (IVR). I. Coherence Effects. *J. Chem. Phys.* **1985**, *82* (7), 2961–2974. <https://doi.org/10.1063/1.448246>.
- (46) Felker, P. M.; Zewail, A. H. Dynamics of Intramolecular Vibrational-energy Redistribution (IVR). II. Excess Energy Dependence. *J. Chem. Phys.* **1985**, *82* (7), 2975–2993. <https://doi.org/10.1063/1.448247>.
- (47) Pettersson, M.; Maçôas, E. M. S.; Khriachtchev, L.; Fausto, R.; Räsänen, M. Conformational Isomerization of Formic Acid by Vibrational Excitation at Energies below the Torsional Barrier. *J. Am. Chem. Soc.* **2003**, *125* (14), 4058–4059. <https://doi.org/10.1021/ja0295016>.
- (48) Duarte, L. J.; Nunes, C. M.; Fausto, R.; Braga, A. A. C. A Protocol for the Investigation of the Intramolecular Vibrational Energy Redistribution Problem: The Isomerization of Nitrous Acid as a Case of Study. *Phys. Chem. Chem. Phys.* **2025**, *27* (7), 3685–3700. <https://doi.org/10.1039/D4CP04130E>.
- (49) Nunes, C. M.; Doddipatla, S.; Loureiro, G. F.; Roque, J. P. L.; Pereira, N. A. M.; Pinho E Melo, T. M. V. D.; Fausto, R. Differential Tunneling-Driven and Vibrationally-Induced Reactivity in Isomeric Benzazirines. *Chem. – Eur. J.* **2022**, *28* (67), e202202306. <https://doi.org/10.1002/chem.202202306>.
- (50) Akai, N.; Kudoh, S.; Nakata, M. Photoisomerization and Tunneling Isomerization of Tetrachlorohydroquinone in a Low-Temperature Argon Matrix. *J. Phys. Chem. A* **2003**, *107* (19), 3655–3659. <https://doi.org/10.1021/jp0225065>.
- (51) Lopes, S.; Domanskaya, A. V.; Fausto, R.; Räsänen, M.; Khriachtchev, L. Formic and Acetic Acids in a Nitrogen Matrix: Enhanced Stability of the Higher-Energy Conformer. *J. Chem. Phys.* **2010**, *133* (14), 144507. <https://doi.org/10.1063/1.3484943>.
- (52) Krupa, J.; Wierzejewska, M.; Lundell, J. Matrix Isolation FTIR and Theoretical Study of Weakly Bound Complexes of Isocyanic Acid with Nitrogen. *Molecules* **2022**, *27* (2), 495. <https://doi.org/10.3390/molecules27020495>.
- (53) Roque, J. P. L.; Nunes, C. M.; Schreiner, P. R.; Fausto, R. Hydrogen Tunneling Exhibiting Unexpectedly Small Primary Kinetic Isotope Effects. *Chem. – Eur. J.* **2024**, *30* (39), e202401323. <https://doi.org/10.1002/chem.202401323>.
- (54) Lopes Jesus, A. J.; Fausto, R.; Reva, I. Conformational Space, IR-Induced, and UV-Induced Chemistry of Carvacrol Isolated in a Low-Temperature Argon Matrix. *J. Phys. Chem. A* **2021**, *125* (37), 8215–8229. <https://doi.org/10.1021/acs.jpca.1c05907>.
- (55) Lopes Jesus, A. J.; Nunes, C. M.; Reva, I. Conformational Structure, Infrared Spectra and Light-Induced Transformations of Thymol Isolated in Noble Gas Cryomatrices. *Photochem* **2022**, *2* (2), 405–422. <https://doi.org/10.3390/photochem2020028>.



- (56) Akai, N.; Kudoh, S.; Takayanagi, M.; Nakata, M. Cis–Trans Isomerization Equilibrium in Hydroquinone in Low-Temperature Argon and Xenon Matrices Studied by FTIR Spectroscopy. *Chem. Phys. Lett.* **2002**, *356* (1–2), 133–139. [https://doi.org/10.1016/S0009-2614\(02\)00379-2](https://doi.org/10.1016/S0009-2614(02)00379-2).
- (57) Quesada-Moreno, M. M.; Krin, A.; Schnell, M. Analysis of Thyme Essential Oils Using Gas-Phase Broadband Rotational Spectroscopy. *Phys. Chem. Chem. Phys.* **2019**. <https://doi.org/10.1039/c9cp05583e>.
- (58) Schmitz, D.; Shubert, V. A.; Giuliano, B. M.; Schnell, M. The Broadband Microwave Spectra of the Monoterpenoids Thymol and Carvacrol: Conformational Landscape and Internal Dynamics. *J. Chem. Phys.* **2014**, *141* (3), 034304. <https://doi.org/10.1063/1.4887337>.
- (59) Pinillos, P.; Torres-Hernández, F.; Usabiaga, I.; Pinacho, P.; Fernández, J. A. Exploration of Carvacrol Aggregation by Laser Spectroscopy. *Phys. Chem. Chem. Phys.* **2024**, *26* (37), 24533–24541. <https://doi.org/10.1039/D4CP02945C>.
- (60) Becke, A. D. Density-functional Thermochemistry. III. The Role of Exact Exchange. *J. Chem. Phys.* **1993**, *98* (7), 5648–5652. <https://doi.org/10.1063/1.464913>.
- (61) Wu, Q.; Yang, W. Empirical Correction to Density Functional Theory for van Der Waals Interactions. *J. Chem. Phys.* **2002**, *116* (2), 515–524. <https://doi.org/10.1063/1.1424928>.
- (62) Vosko, S. H.; Wilk, L.; Nusair, M. Accurate Spin-Dependent Electron Liquid Correlation Energies for Local Spin Density Calculations: A Critical Analysis. *Canadian Journal of Physics*. 58th ed. 1980, pp 1200–1211.
- (63) Stephens, P. J.; Devlin, F. J.; Chabalowski, C. F.; Frisch, M. J. Ab Initio Calculation of Vibrational Absorption and Circular Dichroism Spectra Using Density Functional Force Fields. *J. Phys. Chem.* **1994**, *98* (45), 11623–11627. <https://doi.org/10.1021/j100096a001>.
- (64) Barone, V. Anharmonic Vibrational Properties by a Fully Automated Second-Order Perturbative Approach. *J. Chem. Phys.* **2005**, *122* (1), 014108. <https://doi.org/10.1063/1.1824881>.
- (65) Barone, V.; Bloino, J.; Guido, C. A.; Lipparini, F. A Fully Automated Implementation of VPT2 Infrared Intensities. *Chem. Phys. Lett.* **2010**, *496* (1–3), 157–161. <https://doi.org/10.1016/j.cplett.2010.07.012>.
- (66) Barone, V.; Biczysko, M.; Bloino, J. Fully Anharmonic IR and Raman Spectra of Medium-Size Molecular Systems: Accuracy and Interpretation. *Phys Chem Chem Phys* **2014**, *16* (5), 1759–1787. <https://doi.org/10.1039/C3CP53413H>.
- (67) Frisch, M. J.; Trucks, G. W.; Schlegel, H. B.; Scuseria, G. E.; Robb, M. A.; Cheeseman, J. R.; Scalmani, G.; Barone, V.; Petersson, G. A.; Nakatsuji, H.; Li, X.; Caricato, M.; Marenich, A. V.; Bloino, J.; Janesko,



B. G.; Gomperts, R.; Mennucci, B.; Hratchian, H. P.; Ortiz, J. V.; Izmaylov, A. F.; Sonnenberg, J. L.; Williams-Young, D.; Ding, F.; Lipparini, F.; Egidi, F.; Goings, J.; Peng, B.; Petrone, A.; Henderson, T.; Ranasinghe, D.; Zakrzewski, V. G.; Gao, J.; Rega, N.; Zheng, G.; Liang, W.; Hada, M.; Ehara, M.; Toyota, K.; Fukuda, R.; Hasegawa, J.; Ishida, M.; Nakajima, T.; Honda, Y.; Kitao, O.; Nakai, H.; Vreven, T.; Throssell, K.; Montgomery, J. A., Jr.; Peralta, J. E.; Ogliaro, F.; Bearpark, M. J.; Heyd, J. J.; Brothers, E. N.; Kudin, K. N.; Staroverov, V. N.; Keith, T. A.; Kobayashi, R.; Normand, J.; Raghavachari, K.; Rendell, A. P.; Burant, J. C.; Iyengar, S. S.; Tomasi, J.; Cossi, M.; Millam, J. M.; Klene, M.; Adamo, C.; Cammi, R.; Ochterski, J. W.; Martin, R. L.; Morokuma, K.; Farkas, O.; Foresman, J. B.; Fox, D. J. Gaussian~16 Revision C.01, 2016.

- (68) Schmitz, D.; Shubert, V. A.; Giuliano, B. M.; Schnell, M. The Broadband Microwave Spectra of the Monoterpenoids Thymol and Carvacrol: Conformational Landscape and Internal Dynamics. *J. Chem. Phys.* **2014**, *141* (3), 034304. <https://doi.org/10.1063/1.4887337>.



Data Availability Statement

The authors confirm that the data supporting the findings of this study are available within the article and its supplementary materials. All data necessary for reproducing the calculations, including optimized structures, are presented in the supplementary information material, where the reader can also find figures with experimental data supporting our findings. All data gathered during the experiments are available from the corresponding author, AJLJ, or the author LJD, upon request.

